buildings

MDPI

Article

Experimental Investigation on the Influence of Strength Grade on the Surface Fractal Dimension of Concrete under Sulfuric Acid Attack

Jie Xiao [1], Hehui Zeng [1], Huanqiang Huang [1], Lingfei Liu [2], Long Li [3,*], Bingxiang Yuan [1] and Zucai Zhong [4]

1 School of Civil and Transportation Engineering, Guangdong University of Technology, Guangzhou 510006, China; xiaojie2017@gdut.edu.cn (J.X.); 2112209115@mail2.gdut.edu.cn (H.Z.); 2112209117@mail2.gdut.edu.cn (H.H.); yuanbx@gdut.edu.cn (B.Y.)
2 School of Transportation, Civil Engineering & Architecture, Foshan University, Foshan 528225, China; lingfeiliu@fosu.edu.cn
3 College of Civil Engineering, Tongji University, Shanghai 200092, China
4 Guangdong Sanhe Building Materials Group Co., Ltd., Zhongshan 528414, China; taojiangxiaojie@126.com
* Correspondence: longli@tongji.edu.cn

Abstract: The corrosion of alkaline concrete materials exposed to a sulfuric acid environment is becoming more and more prevalent, and its damage assessment is becoming more and more imperative. This study aims to describe the corroded surfaces of concrete with different strength grades (C30, C50, C80) in sulfuric acid environments in terms of their three-dimensional fractal dimension. Three kinds of concrete with varying strength grades, namely C30, C50, and C80, were immersed in a sulfuric acid solution with pH $\approx$ 0.85 for four distinct corrosion durations, specifically 0, 28, 56, and 165 days, in accelerated corrosion tests. The 3D laser scanning technique was utilized to capture the 3D coordinates of the surface points of the concrete cylinder before and after corrosion. The fractal dimension of concrete's uneven surface before and after corrosion was computed via the cube covering method, and the mass loss of the concrete specimen was also obtained. The outcomes demonstrate that the three-dimensional fractal dimension provides a new method for characterizing the degree of corrosion deterioration of concrete samples affected by sulfuric acid via laser scanning technology. From the perspective of the appearance, mass loss, and fractal dimension of a rough surface in the sulfuric acid environment at a pH level of approximately 0.85, the degree of the corrosion deterioration of concrete is ranked from high to low as C80 > C50 > C30. These fractal dimensions of the concrete's corroded surfaces with various strength grades increase rapidly in the initial period. However, as the corrosion time progresses, the growth rate of the corroded surface fractal dimension gradually decelerates and tends towards stability, which accords with the law of exponential function. The widespread belief is that the higher the strength grade of concrete, the better its durability; however, this pattern varies in sulfuric acid corrosive environments. Therefore, based on this research, it is recommended that in extremely acidic environments (i.e., very low pH), more attention should be paid to high-strength grades of concrete.

Keywords: durability of concrete; sulfuric acid corrosion; grade of strength; fractal characteristics; mass reduction

check for updates

Citation: Xiao, J.; Zeng, H.; Huang, H.; Liu, L.; Li, L.; Yuan, B.; Zhong, Z. Experimental Investigation on the Influence of Strength Grade on the Surface Fractal Dimension of Concrete under Sulfuric Acid Attack. *Buildings* **2024**, *14*, 713. https://doi.org/10.3390/buildings14030713

Academic Editor: Bjorn Birgisson

Received: 28 December 2023
Revised: 18 February 2024
Accepted: 5 March 2024
Published: 7 March 2024

1. Introduction

Concrete has the advantages of easy-to-obtain local materials, low cost, flexible formulation, and simple construction, and it has become the most extensively studied and used civil engineering material [1–7]. However, concrete structures may suffer from various forms of harsh environmental erosion during their service life, thereby shortening their service life [8,9]. Metha P. K. [10] pointed out in his report titled "Durability of Concrete—Fifty Years of Progress?" that the causes of concrete failure are ranked in descending order of importance: steel corrosion, frost damage in cold climates, and physical and chemical reactions in corrosive environments. Concrete is an alkaline material. If it encounters acidic substances, it will undergo an acid–base neutralization reaction, leading to the decomposition of alkaline calcium hydroxide and cement hydration products, reducing the strength and durability of concrete [11]. It is worth noting that sulfuric acid is among the most dangerous acids acting on concrete materials, as it has a combined effect of acid and sulphate corrosion. In engineering practice, sulfuric acid environments are often encountered, including acid rain [12–14], industrial environments, and sewage treatment systems [15–18]. Therefore, research regarding concrete resistance to sulfuric acid corrosion has attracted more and more attention, and scholars have carried out various explorations. So far, there is no specific standard to evaluate the sulfuric acid resistance of concrete [19,20]. Due to the convenience of testing and intuitive description, most scholars measure the visual appearance [21,22], corrosion depth [23,24], mass loss [25,26], and compressive strength loss [27,28] of concrete test blocks after sulfuric acid corrosion as important indicators of the degree of corrosion. However, less attention has been paid to the variation in surface roughness after concrete corrosion. Multiple studies have shown that surface roughness plays a crucial role in the performance of numerous civil engineering components. The shear behavior of the interface between soil and concrete materials (such as pile foundations, retaining walls, slope protection, dams, etc.) is closely related to the roughness of concrete. Surface roughness is also one of the crucial factors affecting the bonding performance of the interface between the concrete and the rock [29], as well as the contact surface between precast concrete and cast-in-place concrete [30–32]. The change in the roughness of concrete pavement caused by sulfuric-acid-type acid rain can cause driving bumps or slippage [33]. There are several well-known approaches for assessing the surface roughness of concrete. The first method is to determine surface roughness by comparing the prepared surface visually with nine standard concrete surface patterns (CSPs) [34]. Although this approach is efficient and simple to implement, it only provides a qualitative evaluation and lacks quantitative data. The second approach is the sand patch test, which usually surrounds the surface of the specimen with a plastic plate and keeps its top consistent with the highest point of the joint surface. Then, the investigator spreads standard sand on the concrete's surface to evaluate the concrete interface roughness according to the average depth of the sand [35]. However, this method is only applicable to the measurement of horizontal specimens and only describes the average surface depth of specimens, which cannot accurately describe the three-dimensional surface topography characteristics of specimens. The third method is to use a mechanical stylus to evaluate surface roughness under laboratory conditions [36]. However, the accuracy of this method is influenced by factors such as the size of the probe and its movement speed, and there is a risk of surface damage during the measurement.

With scientific and technological development, 3D laser scanning technology [37,38] and fractal theory [39–42] are gradually being used more and more in civil engineering and have achieved more ideal results compared to traditional methods in the evaluation of concrete roughness. Xiao J. et al. [43–45] utilized 3D laser scanning methodologies to acquire the surface morphology of concrete material with strength grade C50 after sulfuric acid corrosion and studied the fractal dimension variation law of the concrete corrosion surface. However, there are more than ten strength grades of concrete in engineering practice, and different parts of construction projects require the use of different strength grades of concrete. Xiao J. et al. did not consider the pattern of surface roughness variation arising due to different strength grades.

The most significant factor affecting the strength grade of concrete is the ratio of water to cement. Under the same cement strength and other conditions, as the water–cement ratio decreases, concrete strength increases, porosity decreases, and corrosion resistance improves. Therefore, the deterioration law of concrete with different water–cement ratios (that is, concrete with different strength grades) in a sulfuric acid environment has gained the interest of numerous researchers. Fattuhi N. I. et al. [46] conducted research on the influence of the water–cement ratio on the corrosion behavior of cement-based materials in sulfuric acid solution by utilizing cement paste samples with various water–cement ratios of 0.26, 0.3, 0.35, and 0.4. The research results showed that with the increase in the water–cement ratio, the specimens' mass loss in sulfuric acid solution decreased. Pavlík V. [47] investigated the influence of the water–cement ratio (W/C = 0.3~0.6) on the corrosion behavior of hydrated cement paste in nitric acid and acetic acid solutions, and he found that as the water–cement ratio decreased, the corrosion rate of cement slurry in acidic solutions decreased. Kawai K. [48] performed an experiment to understand the influence of the flow of fluid, the intensity of sulfuric acid solution, and the difference in the water–cement ratio on the damage to concrete due to sulfuric acid. Hewayde E. et al. [49] adopted mass reduction in concrete specimens as a measure of concrete degradation to study the combined effect of wetting–drying cycles and parameters like water–cement ratio in concrete mixtures on the resistance of concrete to sulfuric acid, and they observed that as the water–cement ratio decreased, the mass loss of concrete samples exposed to a pH = 1.5 sulfuric acid solution increased. House M. et al. [50] conducted a study on the sulfuric acid resistance of concrete with various water-to-cementitious materials ratios by monitoring for alterations in appearance, dynamic elastic modulus, mass, and cross-section area. Witkowska-Dobrev, J. et al. [51] carried out experiments on the response of ordinary concrete with different water–cement ratios to exposure to 10% acetic acid to study the mechanisms of acid damage to agricultural concrete tanks. Capraro, A. P. B. et al. [52] analyzed the influence of water–cement ratios (0.40, 0.50, and 0.65) on exposed concrete in wastewater treatment plants where microorganisms produced sulfuric acid and caused the dissolution of the cement paste matrix, and they employed compressive strength, ultrasonic velocity, electrical insulation, scanning electron microscopy (SEM), and X-ray diffraction (XRD) to monitor the performance degradation of concrete. Based on the above literature review, we can see that there is a problem that needs to be addressed. In previous studies on the impact of sulfuric acid corrosion on the fractal dimension of concrete surfaces, there has been insufficient attention paid to the degradation patterns of concrete with different strength grades.

In this paper, three commonly used grades of concrete specimens (C30, C50, and C80) in terms of compressive strength in engineering practice were exposed to a sulfuric acid solution with a pH value of approximately 0.85 to carry out accelerated corrosion tests in order to explore the law of the influence of strength grade on concrete appearance, mass reduction, and the fractal characteristics of corroded surfaces under sulfuric acid conditions. The research results are expected to provide a reference for the selection of concrete strength grades under sulfuric acid conditions.

2. Experimental Design and Evaluation Methods

2.1. Experimental Design

The cement utilized in this project is Portland cement (42.5PIIR), which is manufactured by China Resources Cement Holdings Limited. The density is 3100 kg/m^3, the initial setting duration is 116 min, the final setting duration is 178 min, and the specific surface area is 340 m^2/kg. The coarse aggregate is made of granite gravel with a crushing value of 8%, and the fine aggregate is made of machine-made sand with a fineness modulus of 3.0. Concrete with a strength grade of C80 is commonly used in concrete pipe piles. Therefore, the C80 concrete specimens have a mix proportion that is identical to that utilized in a PHC pipe pile factory located in Guangdong Province, where the specimens were formed and cured. Concrete with strength grades of C50 and C30 are commonly used in engineering structures. The specimens of C50 and C30 concrete are poured at a mixing facility located close to the PHC pipeline plant. Naphthalene-based high-efficiency water-reducing agents are added to achieve good working performance. The mixture proportions of concrete specimens with varying strength grades, including C30, C50, and C80, are shown in Table 1. A high-speed centrifugal compaction process is adopted in the processing of the production of pipe piles, and a significant amount of residual slurry will be produced during the pipe piles molding process. The main components of the residual slurry are water, cement, mineral admixtures, fine sand, admixtures, etc. The residual slurry is made up of approximately 70% liquid and 30% solid components. In combination with policy requirements such as energy conservation and emission reduction, the pipe pile enterprise has mixed residual slurry into C80 and C50 concrete products after many years of mixture proportions allocation tests and has realized positive economic and environmental outcomes.

Table 1. Composition ratios of C30, C50 and C80 concretes (kg/m^3).

Strength Grade	Cement	Fly Ash	Mineral Powder	Ground Sand	Sand	Gravel	Superplasticizer	Residual Slurry	Water
C30	198	66	66	/	780	1075	10.8	/	155.0
C50	255	/	/	135	750	1300	9.5	150	/
C80	255	/	/	135	720	1330	9.5	180	/

The coarse aggregate is composed of granite gravel with a continuous gradation of 5–25 mm in size. Table 2 exhibits the particle sieving test of gravel (coarse aggregates) employed in this mixture. Fine aggregate is composed of machine-made sand with a stone powder content of 4%. Table 3 exhibits the particle sieving test of machine-made sand (fine aggregates) employed in this mixture.

Table 2. Sieving test outcomes for granite gravel.

Sieve size (mm)	31.5	26.5	19.0	16.0	9.5	4.75	2.36	<2.36
Grader retained (%)	0	2.5	18.0	46.7	24.5	5.0	2.8	0.5
Accumulated retained (%)	0	2.5	20.5	67.2	91.7	96.7	99.5	100

Table 3. Sieving test outcomes for machine-made sand.

Sieve size (mm)	4.75	2.36	1.18	0.6	1.3	0.15	<0.15
Grader retained (%)	0	21.6	20.0	16.8	19.6	9.6	12.4
Accumulated retained (%)	0	21.6	41.6	58.4	78.0	87.6	100

Concrete with specified compressive strengths of C30, C50, and C80 is poured using cylindrical plastic molds with a diameter of 100 mm and a height of 200 mm. To speed up the corrosion, all samples were submerged in a sulfuric acid solution with a pH value of approximately 0.85 after 28 days of the curing period. The experimental design outline is presented in Table 4.

Table 4. Specimens' organization.

Specimens Shape	Concrete Grade Strength	The Value of pH	Quantity	Immersion Method
cylinders	C30	0.85	12	Total submersion
cylinders	C50	0.85	12	Total submersion
cylinders	C80	0.85	12	Total submersion

Note: Each group has three identical test specimens, and the experimental result represents the mean value of the three specimens in the group.

The sulfuric acid corrosion test of concrete was carried out by the complete immersion method. The cylinder specimen was divided into two layers and completely immersed in a plastic container containing sulfuric acid solution. The liquid level was 50 mm higher than the top surface of the cylinder specimen. The top and bottom of the cylinder specimen were encased in paraffin wax, while its side was left exposed to sulfuric acid, as shown in Figure 1.

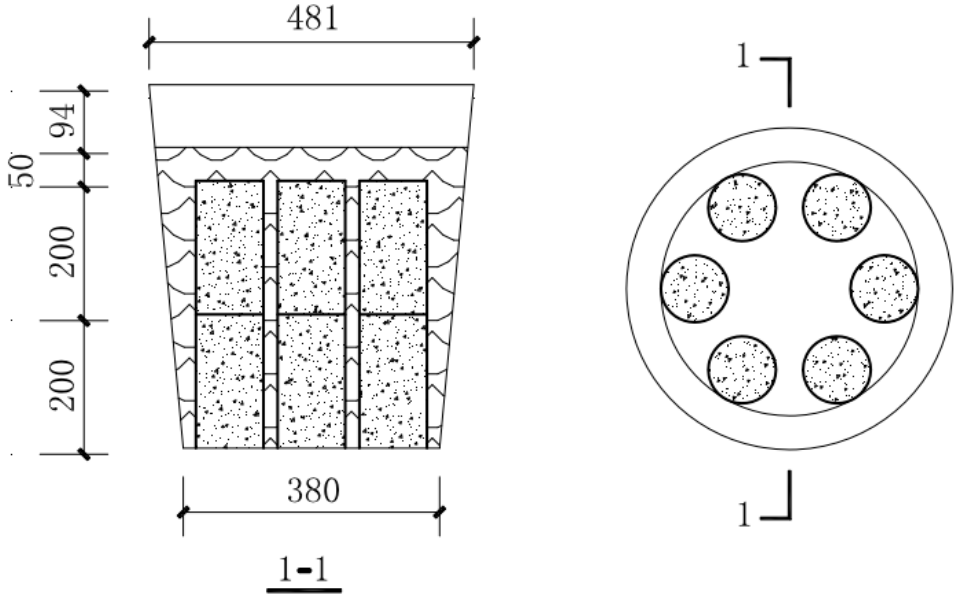

(**a**) front view (**b**) top view

Figure 1. Specimens positioning for sulfuric acid accelerated corrosion test (mm).

2.2. Test Methodologies

2.2.1. The Calculation Method of Mass Loss

In order to obtain a significant corrosion effect within half a year, the specimens were completely immersed in a sulfuric acid solution with pH $\approx$ 0.85. The corrosion durations specified in this paper were 0, 28, 56, and 165 days. During 165 days of immersion periods, the pH of the solution was measured using a Thunder magnetic PHB-4 portable digital acidity meter (0.01 accuracy). The pH of the corrosion solution is adjusted daily by using 98% concentrated sulfuric acid to maintain the pH between 0.83 and 0.87. After the daily addition of concentrated sulfuric acid, the solution is stirred thoroughly with a plastic stick to minimize acid concentration variations in the container. After immersion, the solution is removed from the sulfuric acid solution regularly (after 0, 28, 56, and 165 days) and dried in an oven. An electronic weighing device with a resolution of 1 g and a capacity range of 30 kg are utilized to measure the weight of each specimen before and after corrosion. The loss in mass of a cylindrical specimen is determined using the following formula:

$$K_{mi} = (m_i - m_0)/m_0 \times 100\% \quad (1)$$

where K_{mi} is the percentage of mass loss, %, m_0 and m_i represent the mass of the cylindrical specimen before corrosion and after i days of corrosion, respectively, in kg.

2.2.2. The Calculation Method of Surface Fractal Dimensions

With the advancement of science and technology, portable, high-precision, non-contact 3D laser scanning instruments, coupled with powerful algorithms and data processing software, are becoming increasingly user-friendly and attractive. In this paper, T-SCAN CS, a portable 3D laser scanner manufactured by Steinbichler, Germany, is used as a means of extracting the surface topography of sulfuric-acid-etched concrete. The 3D laser instrument equipment consists of three parts: a spatial positioning receiving system, a computer-controlled acquisition system, and a handheld laser scanner, as shown in Figure 2. There are a total of eight antenna devices on the three surfaces of the handheld laser scanner for transmitting signals. The spatial positioning receiving system can precisely locate the position of the handheld laser scanner in space by receiving the signals sent by the handheld laser scanner so that the surface of the measured object can be digitized in the spatial coordinate system and the point cloud data can be obtained. During the scanning process, the scanning results can be displayed in real time on the computer screen, making the operation very intuitive. The technical specifications of T-SCAN hand-held laser scanner in this paper are the same as it in the reference paper [17].

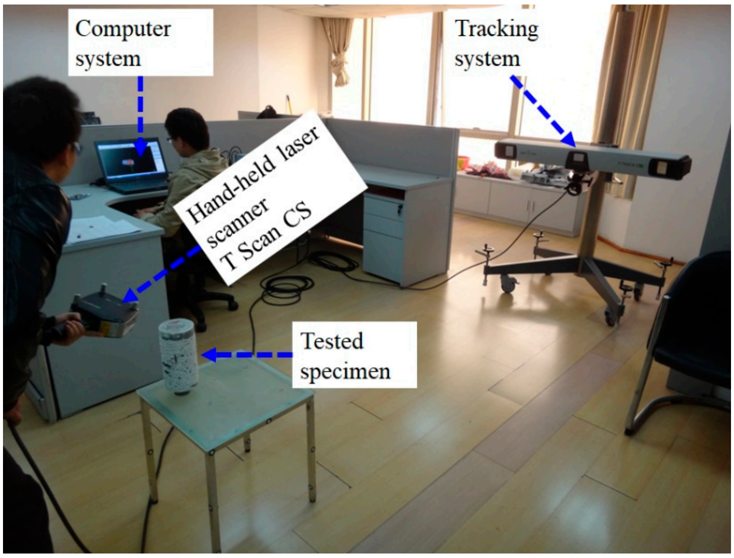

Figure 2. T-SCAN CS 3D laser scanner.

Before laser scanning testing, the T-SCAN CS equipment is calibrated and validated to ensure the reliability of the scanner's effective measurement range and accuracy. The corrosion products on the corroded surface of the concrete sample produced by sulfuric acid attack are gently brushed with a soft brush and then placed on the table. A hand-held laser scanner was used to scan the cylindrical specimen in a circular pattern from top to bottom at a uniform speed until a complete laser scanning image of the corroded cylinder specimen was displayed on the acquisition computer screen. As shown in Figure 3, by comparing the actual morphology of concrete specimens with four different corrosion days and the three-dimensional geometric model captured by laser scanner, it can be seen that the laser scanning technology can effectively obtain the corrosion morphology of concrete specimens.

After the laser scanning of each specimen, the software GOM 2019 Inspect Suite can export the three-dimensional coordinate measurement points of the corroded surface, and the exported file can be read into MATLAB for further processing. MATLAB is used to read the three-dimensional coordinates of the points obtained by laser scanning and then rotate the cylinder until its axis is basically parallel to the Y-axis. Then, the paraffin wax-coated part of the cylinder (the top and bottom cylinder faces and the cylinder faces within the height range of 5 mm near the end faces) is removed, and only the cylinder surface is retained, as displayed in Figures 4 and 5. Then, the corrosion cylinder surface of about 190 mm in height is unfolded into a rectangle in MATLAB, as shown in Figure 6.

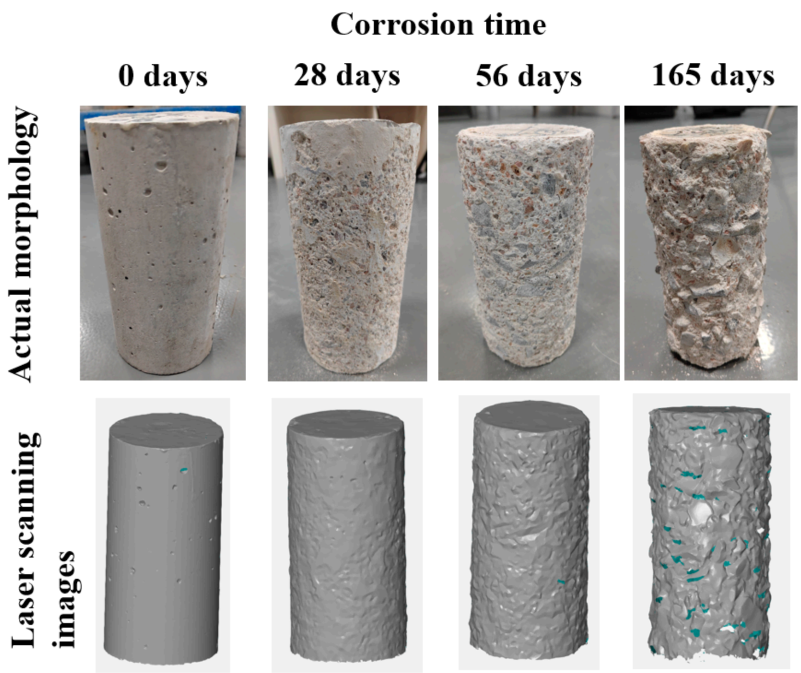

Figure 3. Actual appearance and 3D laser scanning images of the deteriorated concrete.

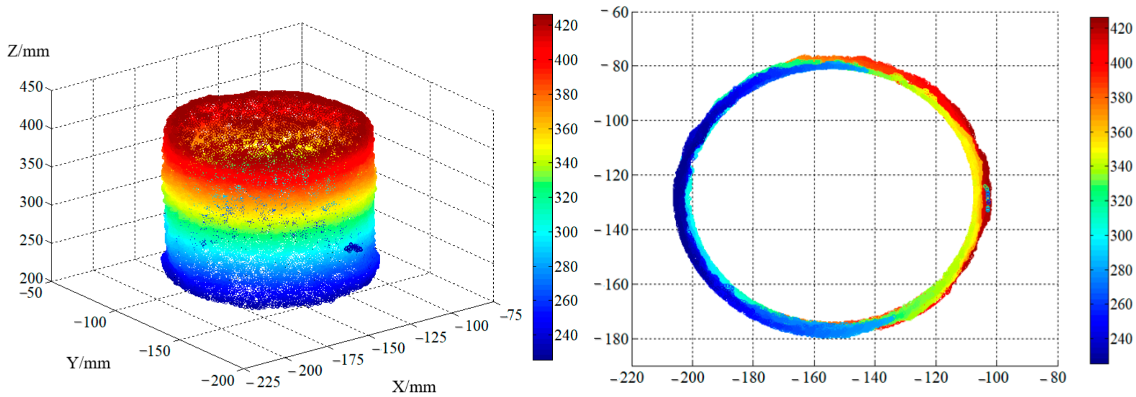

(**a**) axonometric drawing

(**b**) top view

Figure 4. The reconstructed residual cylindrical surface of the cylinder in MATLAB.

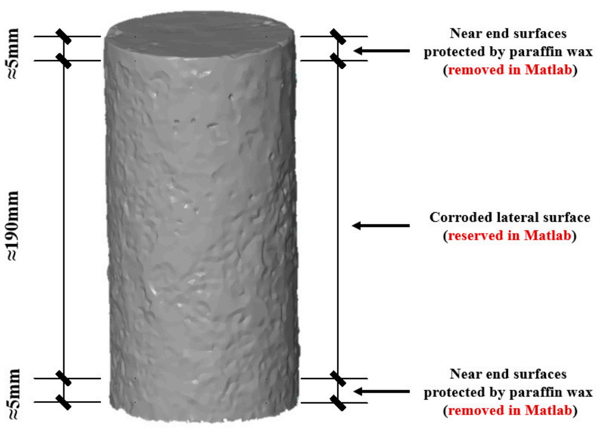

Figure 5. Removing the end face of a cylinder and leaving a cylindrical surface about 190 mm high.

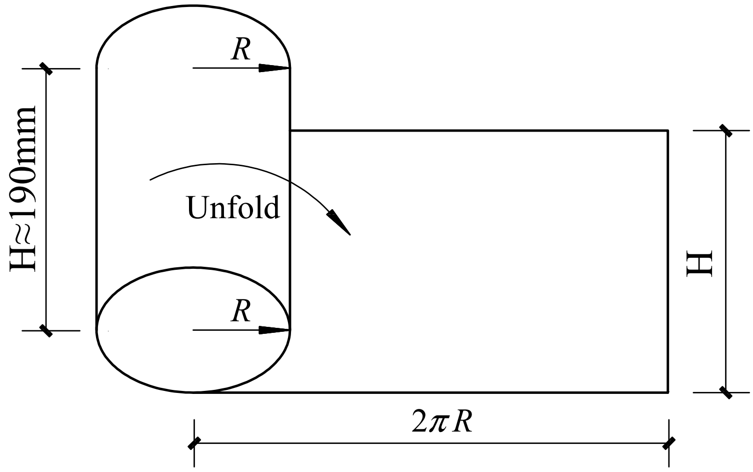

Figure 6. Schematic diagram of unfolding a cylindrical surface into a rectangular plane.

A brief introduction on how to use the cube covering technique to determine the fractal dimension of the unfolded corroded cylindrical surface will be described as follows. In classical Euclidean geometry, the topological dimensions are all integers, such as dots, lines, flat surfaces, and volumes with topological dimensions 0, topological dimensions 1, topological dimensions 2, and topological dimensions 3, respectively. From the perspective of fractal dimensions, lines are one-dimensional, and planes are two-dimensional. For curves on a plane, their dimensions should be between 1 and 2, indicating that the properties of the curve lie between lines and planes, while the dimension of the surface should be between 2 and 3. This expands the concept of “dimension” from integers to fractions, which is known as the “fractal dimension”. “How long is the coastline of the British?” The answer depends on the ruler used. In 1967, Mandelbrot B. B. [53], who pioneered fractal geometry (where dimensions cannot be integers), proposed this interesting question in the journal *Science*. After decades of development, the fractal dimension has proved to be a convenient and reliable tool for evaluating roughness and the irregularity of surfaces and interfaces, and much meaningful progress has been made in this field of study. In the past, most of the methods used to evaluate rough surfaces in fractal dimensions focused on the fractal description of the profile topography on rough surfaces. However, in reality, the topography of rough surfaces is usually very complex, which is manifested by the variability, anisotropy, and local characteristics in spatial distributions. The fractal dimension of a certain section line or the average fractal dimension of several section lines on a rough surface cannot describe the topography of the whole surface [54]. The cubic covering technique developed by Zhou [41] was employed in this article, which can overcome the above shortcomings to calculate the fractal dimension of corroded rough surfaces. The calculation principle of the cube coverage method is the same as it is in the reference paper [45] written by our research group.

3. Experimental Results and Analysis

When the concrete is attacked by sulfuric acid, sulfuric acid will generally react with the alkaline substances in the concrete as follows [25]:

$$\mathrm{Ca}(OH)_2 + H_2SO_4 \rightarrow CaSO_4 \cdot 2H_2O \tag{2}$$

$$\mathrm{CaSiO_2} \cdot 2H_2O + H_2SO_4 \rightarrow CaSO_4 + Si(OH)_4 + H_2O \tag{3}$$

$$3\mathrm{CaO} \cdot Al_2\mathrm{O}_3 \cdot 12H_2O + 3(CaSO_4 \cdot 2H_2O) + 14H_2O \rightarrow 3CaO \cdot Al_2\mathrm{O}_3 \cdot 3CaSO_4 \cdot 32H_2O \tag{4}$$

From the above chemical reaction equation, it can be seen that sulfuric acid not only corrodes concrete with sulfate ions but also has a dissolving effect caused by hydrogen ions. After the reaction between concrete and sulfuric acid, the main reaction product on the surface is gypsum with expansive properties. The further reaction of gypsum in corrosion products and calcium aluminate phases in the cementitious matrix can form more expansive ettringite. Gypsum and ettringite can cause tensile stress in concrete, leading to cracking and peeling. In addition, the generated corrosion products are loose, soft, non-adhesive, and flesh-like, resulting in the surface of the specimen becoming gelatinous and softening.

3.1. Visual Appearance

It is generally believed that the change in visual appearance and shape of concrete cylinder specimens can provide a direct indication of sulfuric acid corrosion severity. Figure 7 shows photographs of concrete cylindrical specimens of specified strengths (C30, C50, and C80) being tested for sulfuric acid resistance for 0, 28, 56, and 165 days. From the photograph, it can be seen that the concrete cylindrical specimens of C80 are severely degraded, while the concrete cylindrical specimens of C30 appear to be slightly damaged near the surface and edges of the specimens. When the concrete cylindrical specimen is not affected by sulfuric acid solution, all specimens with strengths of C30, C50, and C80 have a gray appearance, and the outside is smooth and flat. In the initial period of immersion, the surfaces of concrete cylindrical specimens in the sulfuric acid solution begin to be covered with white sediment. As the corrosion time increases, the sediment thickness increases and expands until it peels off. Following 28 days of sulfuric acid exposure, the cement paste on the surface of the concrete with strength grade C80 was gradually dissolved, and the surface sand was obviously exposed. However, a loose and porous corrosion layer was deposited on the surface of the concrete with strength grade C50, and just a very thin layer of white corrosion product crystals was deposited on the surface of the concrete with strength grade C30. After 165 days of sulfuric acid immersion, the concrete specimens of specified strengths C30 and C50 were not sufficient for the larger aggregates to be detached, while concrete specimens with strength grades C80 showed a large coarse aggregate detachment on the surface. In addition, the cement pastes on the surfaces of C50 and C80 were mainly dissolved and peeled off, and the aggregates were clearly visible, making the surface very rough and uneven, while the coarse aggregates were still not visible on the surface of C30 concrete. From the perspective of appearance, in a sulfuric acid solution with a pH of approximately 0.85, the degree of concrete corrosion deterioration in descending order is C80 > C50 > C30, indicating that the higher the strength grade of concrete, the greater the degree of concrete corrosion deterioration.

3.2. Mass Loss

Mass loss is one of the most widely used indexes to evaluate the intensity of concrete deterioration under sulfuric acid attack because of its convenient testing and simple calculation. Figure 8 demonstrates trend lines of the mass reduction of concrete specimens with strength grades C30, C50, and C80 exposed to a sulfuric acid solution with a pH of approximately 0.85 over a period of 165 days. It becomes apparent from Figure 8 that the percentage of mass reduction of concrete in the initial stage of corrosion is positive, which indicates that the mass has increased. The reason may be due to the reaction between hydrogen ions in the acid solution and the surface of the concrete, resulting in the formation of soluble products and a decrease in mass. However, at the same time, sulfate ions react with hydration products such as calcium hydroxide and tricalcin aluminate, resulting in ettringite and gypsum, which fill the pores of the concrete, resulting in an increase in mass. Moreover, the hydration process of concrete in the acid solution continues, which also causes the mass increase. Therefore, the initial sulfate ion and hydration effects increase the mass, and hydrogen ion has a reducing effect on the mass. However, the former has a more significant impact than the latter. During the later part of corrosion, the mass of

C30 concrete specimens kept increasing, whereas the masses of C50 and C80 displayed a downward trend. However, the C50 concrete specimen always had a higher mass than its initial weight, whereas the C80 concrete specimen experienced rapid mass loss. At the end of 165 days of sulfuric acid exposure, the C80 concrete specimen had a −5.07% loss in mass. Since the porosity of the C30 specimen is comparatively large, the corrosion products that have formed are not yet numerous enough to cause cracks and spalling in the concrete. So, the mass of the C30 concrete specimen is still increasing in the late stage. However, the weights of the C50 and C80 concrete specimens experience a decrease as the corrosion products accumulate to a certain degree because the expansion of the degradation products can cause cracking and damage to the concrete, and eventually the degraded concrete will flake off and cause a reduction in mass. From the comparison of the curves in Figure 8, it can be seen that in a sulfuric acid environment with a pH of approximately 0.85, the order of concrete mass loss from high to low is C80 > C50 > C30, indicating that with higher strength grades of concrete, there is a corresponding increase in concrete mass loss.

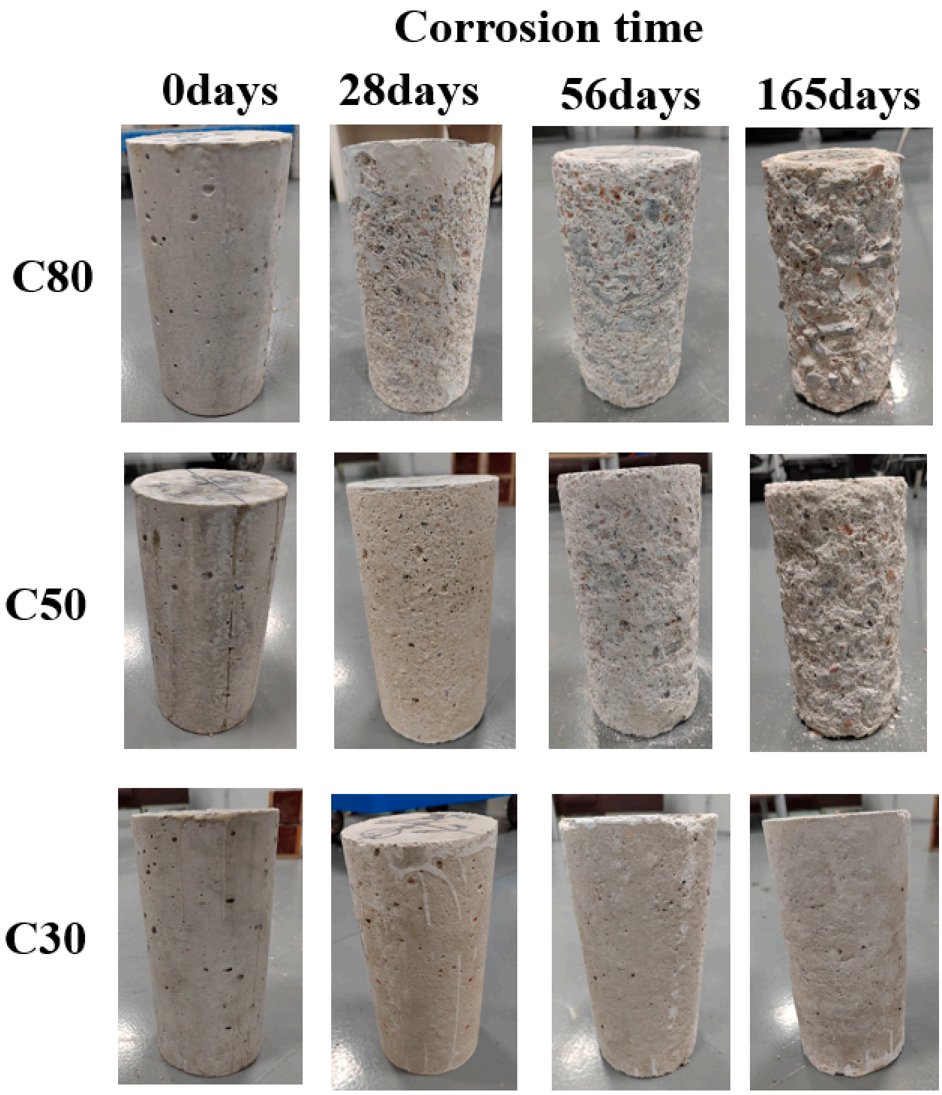

Figure 7. Contrast in the visual appearance of C30, C50, and C80 concrete specimens prior to and following sulfuric acid exposure.

3.3. Fractal Dimension

Taking the concrete cylindrical specimens with a strength grade of C80 and immersed in a sulfuric acid solution with a pH ≈ 0.85 at 0 days, 28 days, 56 days, and 165 days as an example, according to the method described in Section 2.2.2, the three-dimensional coordinates of the points on the corroded surface of concrete obtained by three-dimensional laser scanning are read into MATLAB 2013 software. The two end faces of the cylinder are removed, and only the cylindrical surface is retained. Then, the cylinder surface is expanded into a rectangular surface, as shown in Figure 9.

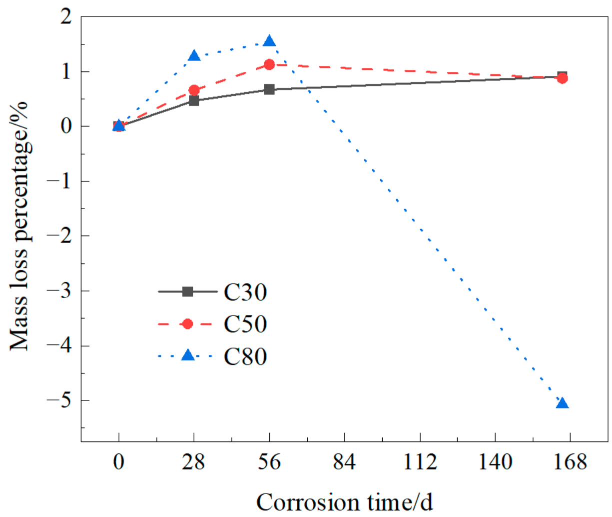

Figure 8. The extent of mass loss changes as the corrosion progresses.

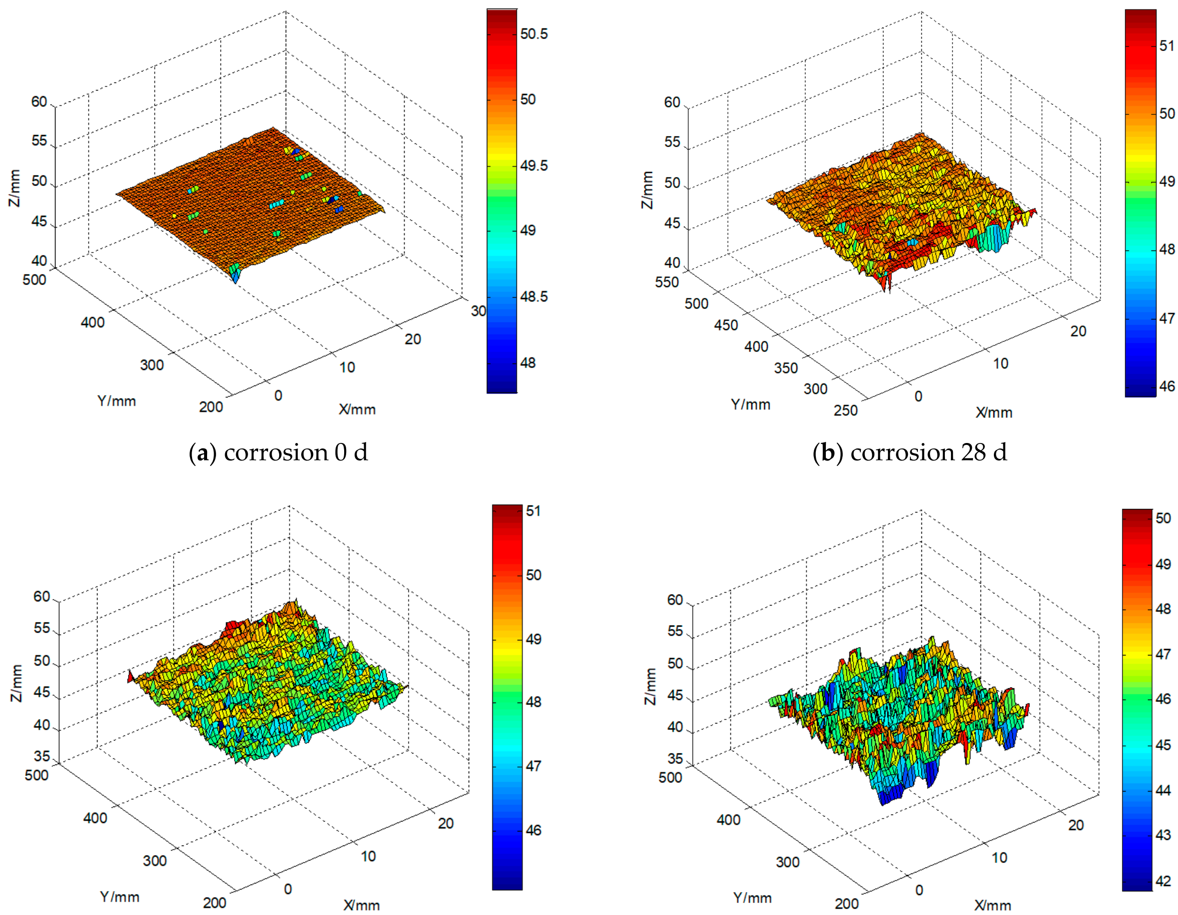

(**a**) corrosion 0 d (**b**) corrosion 28 d

(**c**) corrosion 56 d (**d**) corrosion 165 d

Figure 9. Reconstruction of 190 mm corrosion surface with different corrosion durations in MATLAB.

According to the calculation method of fractal dimensions described in Section 2.2.2, a data processing program was written with MATLAB to calculate the number of $\delta \times \delta$ cubes N(δ) required for each concrete cylinder specimen to cover the rough corrosion surface at different scales δ. Taking the concrete cylindrical specimens with a strength grade of C80 and immersed in a sulfuric acid solution with a pH ≈ 0.85 at 0 days, 28 days, 56 days, and 165 days as an example, the calculated results δ and N(δ) are listed in Table 5. It can be seen from the table that as the side length δ of the cubes decreases, the total number of cubes N(δ) required to cover the corroded rough surface increases. Moreover, when the same side length δ of the cubes is taken, as the corrosion time increases, more cubes N(δ) are needed to cover the corroded rough surface, and as the side length δ of the cube decreases, the corrosion becomes more obvious.

Table 5. Calculation results of δ and N(δ) of the first specimen in each group of concrete with strength grade C80.

Corrosion Duration of Concrete with Strength Grade C80							
0 Days		28 Days		56 Days		165 Days	
δ/mm	N(δ)	δ/mm	N(δ)	δ/mm	N(δ)	δ/mm	N(δ)
2.029	7315	2.011	7301	2.021	7539	1.992	9252
1.004	30,034	0.995	30,623	1.001	36,258	0.986	52,066
0.500	123,372	0.495	147,199	0.498	200,385	0.491	313,535
0.249	506,284	0.247	733,036	0.248	1,059,127	0.245	1,676,567
0.166	1,151,197	0.165	1,795,356	0.165	2,639,044	0.163	4,162,279
0.124	2,061,757	0.123	3,348,331	0.124	4,919,066	0.122	7,742,994
0.100	3,239,310	0.099	5,372,695	0.099	7,916,343	0.098	12,404,301
0.071	6,419,629	0.070	10,863,557	0.071	16,005,575	0.070	25,032,171
0.050	13,239,316	0.049	22,714,698	0.050	33,443,633	0.049	52,093,475

Then, the data are plotted on a log-log coordinate graph (see Figure 10). All the data are almost on the same straight line, and there is a high linear correlation between ln [N(δ)] and ln(δ). It basically follows the function $\ln [N(\delta)] = -D \times \ln(\delta) + C$, where D is the fractal dimension of the required rough corrosion surface, and C is the fitting parameter. According to this method, the fractal dimension D of the corrosion surface of all concrete specimens with strength grades of C30, C50, and C80 was obtained, as shown in Table 6.

Table 6. The fractal dimension D values of different strengths of concrete at different ages (pH ≈ 0.85).

Strength Grade	Corrosion Duration			
	0 Days	28 Days	56 Days	165 Days
C30	2.0252	2.0535	2.1533	2.1368
C50	2.0463	2.1210	2.2707	2.2875
C80	2.0237	2.19744	2.2792	2.3308

Note: The test results were the average value of the test results of each test group including three specimens.

The relationship between the fractal dimension of the corrosion surfaces with strength grades of C30, C50, and C80 in Table 6 and the corrosion time is plotted in Figure 11.

From Figure 11, it can be seen that the fractal dimension of the corroded surface increased rapidly in the early stage, but as the corrosion time extended, the growth rate of the fractal dimension of the corroded surface gradually slowed down and tended to stabilize. This is due to the fact that at the beginning of the corrosion, the cement paste matrix reacted with sulfuric acid and was dissolved to result in the appearance of fine sand grains, which made the fractal dimension D increase rapidly as corrosion time increased. At the later stage of corrosion, on one hand, the dissolution of cement paste increased the pit depth, exposed the aggregates, and increased the fractal dimension D. On the other hand, the debonding of aggregates from the paste would decrease the fractal dimension D.

Under the combined effects of these two actions, the fractal dimension D of the corroded surface grew gradually slower and more stable. From Figure 11, it can be seen that as the corrosion age increases, the fractal dimension D of each strength shows an upward trend before corrosion for 56 days. Moreover, under the same pH solution, the higher the strength grade, the faster the fractal dimension D increases, indicating that the more surface products are generated, the more severe the corrosion is. After 56 days of corrosion, the D value of the C30 specimen showed a decrease due to the gypsum generated in the early stage adhering to the surface of the specimen. As the corrosion continued, the degree of corrosion became more and more severe, and the corrosion layer became thicker. When the corrosion reached a certain degree, the products raised in the outermost layer began to peel off, leading to a certain decrease in roughness, but the overall surface was smoother, and the degree of corrosion was lower. The C50 and C80 specimens continued to increase in fractal dimension, and the higher the strength level, the more the fractal dimension increased, indicating that the higher the strength, the rougher the surface and the more severe the corrosion in pH = 0.85 solution.

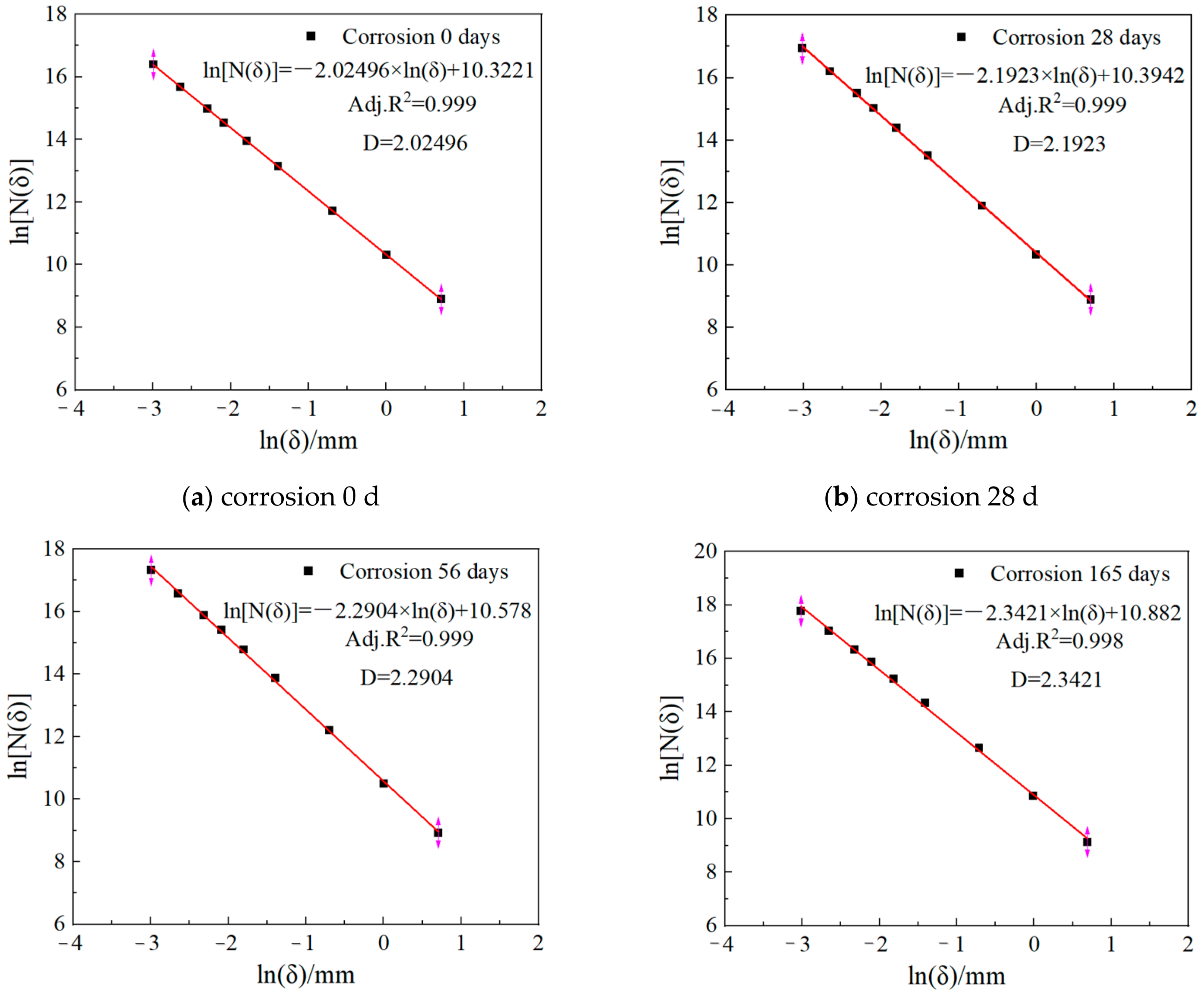

(**a**) corrosion 0 d (**b**) corrosion 28 d (**c**) corrosion 56 d (**d**) corrosion 165 d

Figure 10. Reconstruction of 190 mm corrosion surface of C80 with different corrosion durations in MATLAB.

According to the trend of the fractal dimension of the corroded surface and the corrosion time, the power function, which is widely used to describe corrosion evolution, was chosen to fit the data points in Figure 11. The fitting curve equations between the fractal dimension D of the sulfuric acid corrosion surface of concrete with strength grades of C30, C50, and C80 and the corrosion time t are as follows:

$$D_{C30}(t) = 1.95 \times (t + 7.20)^{0.0193}, Adj.R^2 = 0.73 \tag{5}$$

$$D_{C50}(t) = 1.87 \times (t + 8.80)^{0.0404}, Adj.R^2 = 0.87 \tag{6}$$

$$D_{C80}(t) = 1.98 \times (t + 1.96)^{0.0325}, Adj.R^2 = 0.99 \tag{7}$$

where $D_{C30}(t)$, $D_{C50}(t)$, and $D_{C80}(t)$ are the fractal dimensions of the corrosion surface of concrete with strength grades of C30, C50, and C80 at t days, respectively, and t is the number of corrosion days. It can be seen from the above fitting formulae that the exponents of the power functions of the three fitting formulas are 0.0173, 0.0404, and 0.0325, respectively, all of which are less than 1.0. This indicates that the surface fractal dimension D is positively correlated with the corrosion time t and increases rapidly in the early stage, but the growth rate gradually decreases and tends to be stable in the later stage. As can be seen from Figure 12, the experimental data points and fitting curves are in good agreement, and the goodness of fit is 0.73, 0.87, and 0.99, respectively.

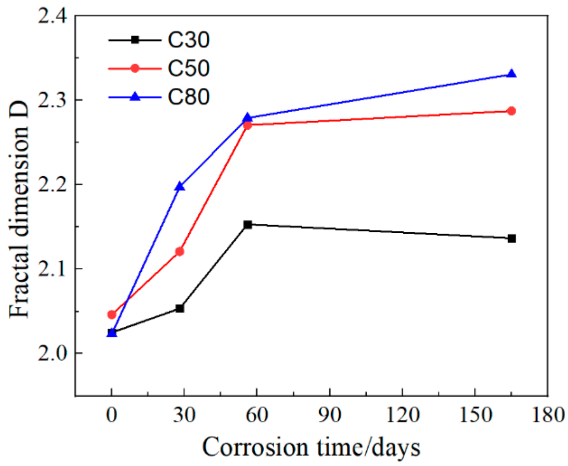

Figure 11. The variation curve of fractal dimension D with values of different concrete strengths with corrosion time.

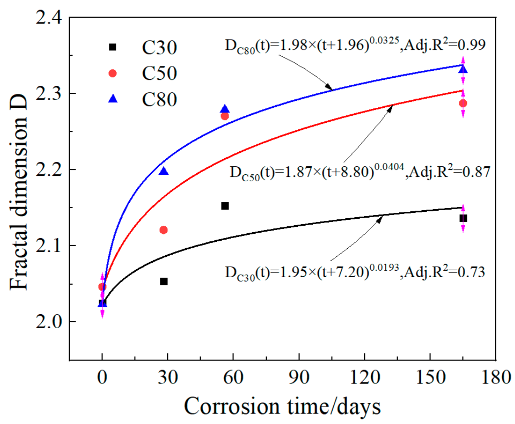

Figure 12. The fitting relationship between fractal dimension D and corrosion time (pH ≈ 0.85).

4. Conclusions

(1) Although previous studies have focused on the performance of concrete exposed to sulfuric acid corrosion under different water–cement ratios, usually using indicators such as corrosion depth, quality loss, and compressive strength to evaluate

the resistance of concrete to sulfuric acid corrosion, the 3D fractal dimension in this paper provides a new method for characterizing the surface roughness of concrete specimens subjected to sulfuric acid corrosion through laser scanning technology.

(2) From the perspective of appearance, in a sulfuric acid environment with pH $\approx$ 0.85, the degree of concrete corrosion deterioration in descending order is C80 > C50 > C30, indicating that the higher the strength grade of concrete, the greater the degree of concrete corrosion deterioration.

(3) From the perspective of mass loss, in a sulfuric acid environment with pH $\approx$ 0.85, the order of concrete mass loss from high to low is C80 > C50 > C30, indicating that the higher the strength grade of concrete, the greater the quality loss of concrete.

(4) The fractal dimension D of each strength shows an upward trend before corrosion for 56 days. Moreover, under the same pH solution, the higher the strength grade, the faster the fractal dimension D increases, indicating that the more surface products are generated, the more severe the corrosion is.

(5) The widespread belief is that the higher the strength grade of concrete, the better its durability. However, the durability varies in sulfuric acid corrosive environments. Therefore, based on the above research, it is recommended that in extremely acidic environments (i.e., very low pH), more attention should be paid to high-strength grades of concrete. In our future work, we plan to further investigate the impact of commonly encountered low-concentration sulfuric acid in practical engineering on the performance degradation of concrete with different strength grades and analyze the mechanism of how the concentration of sulfuric acid affects the experimental results.

Author Contributions: J.X., Z.Z., L.L. (Long Li) and L.L. (Lingfei Liu) played a major role in designing the manuscript. H.H. and H.Z. collected and processed the data. L.L. (Lingfei Liu), H.H. and B.Y. participated in the immersion of the specimens. J.X., L.L. (Long Li) and Z.Z. wrote and revised the paper. All authors have read and agreed to the published version of the manuscript.

Funding: The authors appreciate the funding provided by the National Natural Science Foundation of China with grant no. 52278160 and 51808133 and 52308276 and grant no. 52278336 and 51978177, the Guangdong Basic and Applied Basic Research Foundation with grant no. 2020A1515110814, and the Guangdong Natural Science Foundation with grant no. 2023A1515012081.

Data Availability Statement: The datasets supporting the conclusions of this study are available upon request from the corresponding author.

Acknowledgments: The authors would like to thank all anonymous reviewers for their valuable comments and suggestions. They also express their gratitude to the laboratory at the School of Civil and Transportation Engineering, Guangdong University of Technology, and Guangdong Sanhe Pipe Pile Co., Ltd. for providing the resources required for this research.

Conflicts of Interest: Author Zucai Zhong was employed by the company Guangdong Sanhe Building Materials Group Co., Ltd. The remaining authors declare that the research was conducted in the absence of any commercial or financial relationships that could be construed as a potential conflict of interest.

References

1. Fang, Z.; Wu, J.; Zhao, G.; Fang, S.; Ma, Y.; Jiang, H. Shear performance and design recommendations of single embedded nut bolted shear connectors in prefabricated steel–UHPC composite beams. *Steel Compos. Struct.* **2024**, *50*, 319–336.
2. Feng, J.H.; Shao, X.D.; Qiu, M.H.; Li, H.H.; Gao, X.; Huang, Z.L. Reliability evaluation of flexural capacity design provision for UHPC beams reinforced with steel rebars/prestressing tendons. *Eng. Struct.* **2024**, *300*, 117160. [CrossRef]
3. Jiang, H.B.; Hu, Z.B.; Cao, Z.P.; Gao, X.J.; Tian, Y.Q.; Sun, X.D. Experimental and numerical study on shear performance of externally prestressed precast UHPC segmental beams without stirrups br. *Structures* **2022**, *46*, 1134–1153. [CrossRef]
4. Zhen, H.; Xiong, Z.; Song, Y.; Li, L.; Qiu, Y.; Zou, X.; Chen, B.; Chen, D.; Liu, F.; Ji, Y. Early mechanical performance of glass fibre-reinforced manufactured sand concrete. *J. Build. Eng.* **2024**, *83*, 108440. [CrossRef]
5. Chen, M.; De Corte, W.; Jiang, H.; Taerwe, L. Experimental study on direct-shear behaviour of narrow joints in socket connections for precast pier-to-pile footing systems. *Structures* **2024**, *61*, 106006. [CrossRef]

6. Prakash, R.; Raman, S.N.; Divyah, N.; Subramanian, C.; Vijayaprabha, C.; Praveenkumar, S. Fresh and mechanical characteristics of roselle fibre reinforced self-compacting concrete incorporating fly ash and metakaolin. *Constr. Build. Mater.* **2021**, *290*, 123209. [CrossRef]
7. Jahan, A.; Mollazadeh, M.; Akbarpour, A.; Khatibinia, M. Health monitoring of pressurized pipelines by finite element method using meta-heuristic algorithms along with error sensitivity assessment. *Struct. Eng. Mech.* **2023**, *87*, 211–219. [CrossRef]
8. Shao, W.; Li, Q.M.; Zhang, W.B.; Shi, D.D.; Li, H.H. Numerical modeling of chloride diffusion in cement-based materials considering calcium leaching and external sulfate attack. *Constr. Build. Mater.* **2023**, *401*, 132913. [CrossRef]
9. Shao, W.; Qin, F.; Shi, D.; Soomro, M.A. Horizontal bearing characteristic and seismic fragility analysis of CFRP composite pipe piles subject to chloride corrosion. *Comput. Geotech.* **2024**, *166*, 105977. [CrossRef]
10. Mehta, P.K. Durability of Concrete—Fifty Years of Progress? *ACI Symp. Publ.* **1991**, *126*, 1–32. [CrossRef]
11. Prakash, R.; Thenmozhi, R.; Raman, S.N.; Subramanian, C.; Divyah, N. An investigation of key mechanical and durability properties of coconut shell concrete with partial replacement of fly ash. *Struct. Concr.* **2020**, *22*, E985–E996. [CrossRef]
12. Yu, J.Q.; Qiao, H.X.; Zhu, F.F.; Wang, X.K. Research on Damage and Deterioration of Fiber Concrete under Acid Rain Environment Based on GM(1,1)-Markov. *Materials* **2021**, *14*, 6326. [CrossRef]
13. Yin, Y.S.; Zhang, J.; Zhang, G.H. Effect of hygrothermal acid rain environment on the shear bonding performance of CFRP-concrete interface. *Constr. Build. Mater.* **2023**, *364*, 130002. [CrossRef]
14. Xie, S.D.; Qi, L.; Zhou, D. Investigation of the effects of acid rain on the deterioration of cement concrete using accelerated tests established in laboratory. *Atmos. Environ.* **2004**, *38*, 4457–4466. [CrossRef]
15. Xiao, J.; Qu, W.J.; Jiang, H.B.; Li, L.; Huang, J.; Chen, L. Fractal characterization and mechanical behavior of pile-soil interface subjected to sulfuric acid. *Fractals* **2021**, *29*, 2140010. [CrossRef]
16. Xiao, J.; Qu, W.J.; Li, W.G.; Zhu, P. Investigation on effect of aggregate on three non-destructive testing properties of concrete subjected to sulfuric acid attack. *Constr. Build. Mater.* **2016**, *115*, 486–495. [CrossRef]
17. Xiao, J.; Long, X.; Qu, W.J.; Li, L.; Jiang, H.B.; Zhong, Z.C. Influence of sulfuric acid corrosion on concrete stress-strain relationship under uniaxial compression. *Measurement* **2022**, *187*, 110318. [CrossRef]
18. Monteny, J.; De Belie, N.; Vincke, E.; Verstraete, W.; Taerwe, L. Chemical and microbiological tests to simulate sulfuric acid corrosion of polymer-modified concrete. *Cem. Concr. Res.* **2001**, *31*, 1359–1365. [CrossRef]
19. Mahmoud, M.H.; Bassuoni, M.T. Response of Concrete to Incremental Aggression of Sulfuric Acid. *J. Test. Eval.* **2020**, *48*, 3220–3238. [CrossRef]
20. Girardi, F.; Di Maggio, R. Resistance of concrete mixtures to cyclic sulfuric acid exposure and mixed sulfates: Effect of the type of aggregate. *Cem. Concr. Compos.* **2011**, *33*, 276–285. [CrossRef]
21. Matalkah, F.; Salem, T.; Soroushian, P. Acid resistance and corrosion protection potential of concrete prepared with alkali aluminosilicate cement. *J. Build. Eng.* **2018**, *20*, 705–711. [CrossRef]
22. Nnadi, E.O.; Lizarazo-Marriaga, J. Acid Corrosion of Plain and Reinforced Concrete Sewage Systems. *J. Mater. Civ. Eng.* **2013**, *25*, 1353–1356. [CrossRef]
23. Pavlík, V. Corrosion of hardened cement paste by acetic and nitric acids part I: Calculation of corrosion depth. *Cem. Concr. Res.* **1994**, *24*, 551–562. [CrossRef]
24. Bertron, A.; Duchesne, J.; Escadeillas, G. Accelerated tests of hardened cement pastes alteration by organic acids: Analysis of the pH effect. *Cem. Concr. Res.* **2005**, *35*, 155–166. [CrossRef]
25. Bassuoni, M.T.; Nehdi, M.L. Resistance of self-consolidating concrete to sulfuric acid attack with consecutive pH reduction. *Cem. Concr. Res.* **2007**, *37*, 1070–1084. [CrossRef]
26. Hasan, M.S.; Setunge, S.; Law, D.W.; Molyneaux, T.C.K. Predicting life expectancy of concrete septic tanks exposed to sulfuric acid attack. *Mag. Concr. Res.* **2013**, *65*, 793–801. [CrossRef]
27. Cao, R.Z.; Yang, J.F.; Li, G.X.; Zhou, Q.; Niu, M.D. Durability performance of nano-SiO_2 modified OPC-SAC composites subjected to sulfuric acid attack. *Constr. Build. Mater.* **2023**, *371*, 130802. [CrossRef]
28. Khan, M.N.N.; Elahi, M.M.A.; Kuri, J.C.; Sarker, P.K.; Shaikh, F.U.A. Acid resistance of alkali-activated composites containing waste glass as fine aggregate. *Adv. Cem. Res.* **2022**, *35*, 248–257. [CrossRef]
29. Shen, Y.J.; Wang, Y.Z.; Yang, Y.; Sun, Q.; Luo, T.; Zhang, H. Influence of surface roughness and hydrophilicity on bonding strength of concrete-rock interface. *Constr. Build. Mater.* **2019**, *213*, 156–166. [CrossRef]
30. Chen, L.; Yan, J.; Wu, Z.G.; Yang, D.H.; Li, J.L.; Xiang, N.L. Experimental and numerical study on shear behavior of shear pockets between ultra-high-performance and normal concrete for precast girder bridges. *Structures* **2023**, *55*, 1645–1658. [CrossRef]
31. Mohamad, M.E.; Ibrahim, I.S.; Abdullah, R.; Abd Rahman, A.B.; Kueh, A.B.H.; Usman, J. Friction and cohesion coefficients of composite concrete-to-concrete bond. *Cem. Concr. Compos.* **2015**, *56*, 1–14. [CrossRef]
32. Dai, M.L.; Wang, X.R.; Cheng, C.; Chen, Z.L.; Deng, J.Y. Efficient Evaluation of Concrete Fracture Surface Roughness Using Fringe Projection Technology. *Materials* **2023**, *16*, 4430. [CrossRef] [PubMed]
33. Hu, C.; Zhou, Z.G.; Chen, G.H. Effects of different types of acid rain on water stability of asphalt pavement. *Constr. Build. Mater.* **2022**, *322*, 126308. [CrossRef]
34. Millman, L.R.; Giancaspro, J.W. Three-Dimensional Optical Profilometry Analysis of the International Concrete Repair Institute Concrete Surface Profiles (CSPs). *ACI Mater. J.* **2013**, *110*, 519–527.

35. Sengoz, B.; Topal, A.; Tanyel, S. Comparison of pavement surface texture determination by sand patch test and 3D laser scanning. *Period. Polytech.-Civ. Eng.* **2012**, *56*, 73–78. [CrossRef]
36. Courard, L.; Nelis, M. Surface analysis of mineral substrates for repair works: Roughness evaluation by profilometry and surfometry analysis. *Mag. Concr. Res.* **2003**, *55*, 355–366. [CrossRef]
37. Liu, X.G.; Zhang, W.P.; Gu, X.L.; Ye, Z.W. Assessment of Fatigue Life for Corroded Prestressed Concrete Beams Subjected to High-Cycle Fatigue Loading. *J. Struct. Eng.* **2023**, *149*, 04022242. [CrossRef]
38. Zhang, W.P.; Zhou, B.B.; Gu, X.L.; Dai, H.C. Probability Distribution Model for Cross-Sectional Area of Corroded Reinforcing Steel Bars. *J. Mater. Civ. Eng.* **2014**, *26*, 822–832. [CrossRef]
39. Xue, D.J.; Liu, Y.T.; Zhou, H.W.; Wang, J.Q.; Liu, J.F.; Zhou, J. Fractal Characterization on Anisotropy and Fractal Reconstruction of Rough Surface of Granite Under Orthogonal Shear. *Rock Mech. Rock Eng.* **2020**, *53*, 1225–1242. [CrossRef]
40. Issa, M.A.; Issa, M.A.; Islam, M.S.; Chudnovsky, A. Fractal dimension—A measure of fracture roughness and toughness of concrete. *Eng. Fract. Mech.* **2003**, *70*, 125–137. [CrossRef]
41. Zhou, H.W.; Xie, H. Direct estimation of the fractal dimensions of a fracture surface of rock. *Surf. Rev. Lett.* **2003**, *10*, 751–762. [CrossRef]
42. Zhou, H.W.; Xue, D.J.; Jiang, D.Y. On fractal dimension of a fracture surface by volume covering method. *Surf. Rev. Lett.* **2014**, *21*, 14500152. [CrossRef]
43. Xiao, J.; Long, X.; Li, L.; Jiang, H.; Zhang, Y.; Qu, W. Study on the Influence of Three Factors on Mass Loss and Surface Fractal Dimension of Concrete in Sulfuric Acid Environments. *Fractal Fract.* **2021**, *5*, 146. [CrossRef]
44. Xiao, J.; Xu, Z.; Murong, Y.; Wang, L.; Lei, B.; Chu, L.; Jiang, H.; Qu, W. Effect of Chemical Composition of Fine Aggregate on the Frictional Behavior of Concrete–Soil Interface under Sulfuric Acid Environment. *Fractal Fract.* **2022**, *6*, 22.
45. Xiao, J.; Qu, W.; Jiang, H.; Dong, W. Three-Dimensional Fractal Characterization of Concrete Surface Subjected to Sulfuric Acid Attacks. *J. Nondestruct. Eval.* **2020**, *39*, 57. [CrossRef]
46. Fattuhi, N.I.; Hughes, B.P. The performance of cement paste and concrete subjected to sulphuric acid attack. *Cem. Concr. Res.* **1988**, *18*, 545–553. [CrossRef]
47. Pavlík, V. Corrosion of hardened cement paste by acetic and nitric acids Part III: Influence of water/cement ratio. *Cem. Concr. Res.* **1996**, *26*, 475–490. [CrossRef]
48. Kawai, K.; Yamaji, S.; Shinmi, T. Concrete Deterioration Caused by Sulfuric Acid Attack. In Proceedings of the 10th DBMC International Conference on Durability of Building Materials and Component, Lyon, France, 17–20 April 2005.
49. Hewayde, E.; Nehdi, M.; Allouche, E.; Nakha, G. Effect of mixture design parameters and wetting-drying cycles on resistance of concrete to sulfuric acid attack. *J. Mater. Civ. Eng.* **2007**, *19*, 155–163. [CrossRef]
50. House, M.; Cheng, L.Q.; Banks, K.; Weiss, J. Concrete Resistance to Sulfuric Acid Immersion: The Influence of Testing Details and Mixture Design on Performance as It Relates to Microbially Induced Corrosion. *Adv. Civ. Eng. Mater.* **2019**, *8*, 544–557. [CrossRef]
51. Witkowska-Dobrev, J.; Szlachetka, O.; Francke, B.; Chylinski, F.; Malek, M.; Sadzevieius, R.; Ramukevicius, D.; Frak, M.; Dzieciol, J.; Kruszewski, M.; et al. Effect of different water-cement ratios on the durability of prefabricated concrete tanks exposed to acetic acid aggression. *J. Build. Eng.* **2023**, *78*, 107712. [CrossRef]
52. Capraro, A.P.B.; Cheremeta, M.A.; Gonçalves, M.P.G.; Cremonez, C.; de Medeiros, M.H.F. Influence of the cement type and water/cement ratio in concretes exposed in sewage treatment plants. *Constr. Build. Mater.* **2019**, *229*, 116842. [CrossRef]
53. Mandelbrot, B.B. *The Fractal Geometry of Nature*; W.H. Freeman and Company: New York, NY, USA, 1982.
54. Ai, T.; Zhang, R.; Zhou, H.W.; Pei, J.L. Box-counting methods to directly estimate the fractal dimension of a rock surface. *Appl. Surf. Sci.* **2014**, *314*, 610–621. [CrossRef]